Available online at www.sciencedirect.com
ScienceDirect
Atmospheric Environment 42 (2008) 6405–6416
ATMOSPHERIC ENVIRONMENT
www.elsevier.com/locate/atmosenv

Radiative and dynamic effects of absorbing aerosol particles over the Pearl River Delta, China

M. Wendisch[a,b,*], O. Hellmuth[a], A. Ansmann[a], J. Heintzenberg[a], R. Engelmann[a], D. Althausen[a], H. Eichler[a], D. Müller[a], M. Hu[c], Y. Zhang[c], J. Mao[d]

[a]*Leibniz Institute for Tropospheric Research, Leipzig, Germany*
[b]*Institute for Atmospheric Physics, Johannes Gutenberg-University of Mainz, Germany*
[c]*State Key Joint Laboratory of Environmental Simulation and Pollution Control, College of Environmental Sciences, Peking University, Beijing, China*
[d]*Department of Atmospheric Science, School of Physics, Peking University, Beijing, China*

Received 3 September 2007; received in revised form 8 February 2008; accepted 12 February 2008

Abstract

Results are reported from a ground-based measurement campaign conducted in a highly polluted region in southeast of China in October–November 2004. The experiment focused on absorbing aerosol particles and their effects on the solar radiation field and local meteorology. A Raman lidar in conjunction with Sun photometer data measured profiles of particle extinction; ground-based in situ data of aerosol optical properties were collected by nephelometer and absorption photometer. Exceptionally high values of aerosol optical depth of up to 1.5 were observed.

The measurements were input to a radiative transfer model, which simulated high solar radiative forcing values for the aerosol particles of up to $-160\,W\,m^{-2}$ at the ground (daily average) for the observed particle single-scattering albedo of 0.85. Maximum solar heating rates of 7–8 K day^{-1} were simulated at the top of the aerosol layer.

The radiative simulations were used to drive a dynamic model of the planetary boundary layer (PBL). With this model the temporal course of the height of the PBL was simulated and compared with respective lidar data. The results show that the height of the PBL is significantly decreased due to the warming of the aerosol particles at the top of the PBL. In this way, the stabilizing effect of absorbing aerosol particles within the PBL was confirmed by a combination of experimental and modeling means.

Keywords: Atmospheric radiation; Planetary boundary layer

1. Introduction

Cooling of the lower parts of an atmospheric layer, combined with heating aloft and horizontal flux divergence, leads to increased stability of the layer, reduced vertical air exchange, and (assuming constant aerosol sources at the ground) steady increase of particulate pollution in the layer. This

*Corresponding author at: Institute for Atmospheric Physics, Johannes Gutenberg-University, Becherweg 21, D-55099 Mainz, Germany. Tel.: +49 6131 39 24664; fax: +49 6131 39 23532.
E-mail address: wendisch@uni-mainz.de (M. Wendisch).

1352-2310/$ - see front matter © 2008 Elsevier Ltd. All rights reserved.
doi:10.1016/j.atmosenv.2008.02.033

enhancement of particle concentrations in turn leads to further warming aloft (due to the absorption of solar radiation by the anthropogenic aerosol particles, soot for example), even stronger stability and further delimited vertical mixing in the layer. Thus, a positive feedback is established in which the presence of the pollutant (absorbing particles) enhances its concentration. Such feedback mechanisms have been detected over South Asia and the Indian Ocean (Podgorny et al., 2000; Ramanathan et al., 2001; Krishnan and Ramanathan, 2002; Menon et al., 2002; Ramanathan and Ramana, 2005) and elsewhere (Jacobson, 1998). Suppression of precipitation due to such processes has been hypothesized by Zhao et al. (2006). Further studies have discussed about atmospheric stability (Ramanathan et al., 2005) caused by absorption due to aerosol particles. Rudich et al. (2003) report on increased convection out of the boundary layer into the overlying air induced by aerosol absorption of solar energy. Further effects on regional circulation have been reported by Chung et al. (2002) and on evaporation of boundary layer clouds by Ackerman et al. (2000). Enhanced stability due to aerosols has also been hypothesized to reduce wind speeds (Jacobson and Kaufman, 2006). However, solid experimental validation of these simulation results is still lacking.

In this paper we quantify the link between enhanced aerosol particle absorption and the height of the planetary boundary layer (PBL) by combining observations and simulations. For this purpose we have used comprehensive aerosol measurements performed during an intensive measurement campaign in the Pearl River Delta (PRD), which is located in the Southeast of China. The measurement campaign is called Program of Regional Integrated Experiments of Air Quality over PRD 2004 (PRIDE-PRD2004) in the subsequent text. The scientific focus of PRIDE-PRD2004 was to characterize the pollution status and to investigate the related atmospheric chemical and radiative processes in the PRD, one of the most densely populated and highly polluted regions of Asia (Zhang et al., 2007, submitted for publication). Part of the aerosol data collected during the experiment are combined with sophisticated radiation and columnar meteorological modeling. In particular, we have investigated the influence of the aerosol particles on the evolution of the height of the PBL during one specific measurement day (23 October 2004). The results clearly reveal the significant impact of absorbing aerosol particles on the temporal development of the PBL height.

In Section 2 the methodology is introduced, including a description of the experiment, the instrumentation as well as the radiative and dynamic PBL modeling. Section 3 contains the results obtained with regard to radiative forcing of the aerosol particles in this polluted environment and their influence on PBL height evolution. The conclusions of the paper are summarized in Section 4.

2. Methodology

2.1. Program of Regional Integrated Experiments of Air Quality over PRD 2004 (PRIDE-PRD2004)

The PRD occupies the low-lying areas alongside the Pearl River estuary at the South China Sea. It comprises the central part of the Guangdong Province and reaches from Macao to Guangzhou inland, and via Shenzhen to Hong Kong (see Fig. 1). More than 40 million people are living in less than $30,000\,km^2$ making it the most densely populated and largest urban area in the world with rapid economic growth. The accompanying environmental side effects have been a major concern of local and regional governments for some time.

In order to quantify the impact of high aerosol loads in the PRD a dedicated field experiment (PRIDE-PRD2004) was performed in this area in October–November 2004 (Zhang et al., 2007, submitted for publication). The measurements focused on the vertical distribution of the optical properties of anthropogenic haze and related

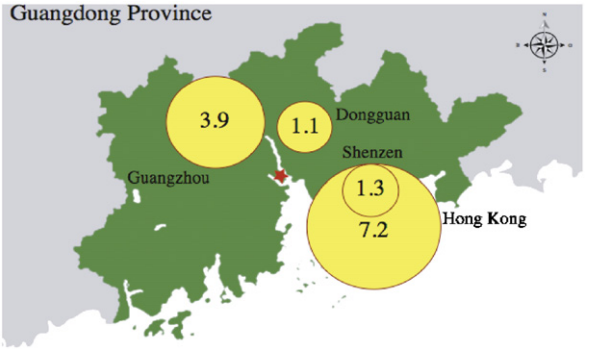

Fig. 1. Map of the Pearl River Delta and population estimates in millions for 2005 in cities with more than 750,000 inhabitants in the year 2005. The field site of the PRD experiment is marked with a star.

meteorological consequences in the PRD. First results were published by Ansmann et al. (2005).

The measurements took place at Xinken (22.6°N, 113.6°E, see star in Fig. 1) on the banks of the Pearl River, about 80 km northwest of Hong Kong, 60 km southeast of Guangzhou, and 50 km west of Shenzen.

Northerly and northeasterly air flows with low wind speeds prevailed in the PRD throughout October–November 2004. The mostly sunny and dry meteorological conditions during this time period allowed almost continuous observations. In particular, stable cloudless synoptic conditions persisted in the time period from 22 to 25 October 2004. This meteorological situation favored the transport of particulate pollution from the Chinese mainland to the PRD and the accumulation of locally produced aerosol particles. A steady aerosol layering was found on 23 and 24 October with stable stratification during nighttime (multiple layers up 2.3 km height) and pronounced PBL development during daytime. Sea breeze effects on both days led to moderately polluted conditions during daytime and stagnant haze at night. Thus, in order to elucidate aerosol effects on PBL evolution, 23 October 2004, was chosen for the detailed evaluation and model study.

Nearby profile measurements of meteorological parameters by radiosondes were not available. This limits our ability to compare the meteorological output of our dynamic model with appropriate measured data. However, our intention is to specifically investigate the impact of enhanced aerosol concentrations on the PBL height. This parameter can be well measured by lidar and thus does not necessarily require radiosonde data.

The height of the PBL was derived from the profile of the lidar particle backscatter coefficient using a wavelet covariance transform algorithm (Brooks, 2003). Several authors have compared lidar-derived PBL height measurements with results obtained from radiosonde profile data (Martucci et al., 2007; Lammert and Bösenberg, 2005). These studies have shown that the lidar-derived PBL heights are in good agreement with the radiosonde data.

The aerosol instrumentation included a Sun photometer (manufactured by Dr. Schulz and Partner GmbH, Buckow, Germany) to measure aerosol optical depth (AOD) at eight wavelengths from 380 to 1044 nm. With a portable Raman lidar (Althausen et al., 2004; Ansmann et al., 2005) profiles of particle volume backscatter and extinction coefficients were measured at 532 nm wavelength. At the surface particles were collected using an aerosol inlet system. During the collection the particles were dried. Respective dry volume scattering and absorption coefficients of the particles were measured downstream of the inlet with an integrating nephelometer (Anderson et al., 1996) and a particle absorption photometer (Petzold et al., 2002). From these data the dry volumetric single-scattering albedo of the aerosol particles was derived. The instruments used in this study are summarized in Table 1.

During the experiment exceptionally high dry particulate mass concentrations were observed at the surface with values up to $300\,\mu g\,m^{-3}$. Grand average AOD values at 532 nm wavelength were 0.92 with a standard deviation of 0.31. In 20% of all measurements AOD values larger than 1.2 were recorded (Ansmann et al., 2005). Between 21 and 24 October, at the surface average aerosol scattering coefficients σ_s of $(0.32 \pm 0.09) \times 10^{-3}\,m^{-1}$ and average particle absorption coefficients σ_a of $(0.06 \pm 0.03) \times 10^{-3}\,m^{-1}$ (both at 550 nm wavelength) were measured with the nephelometer and the absorption photometer, respectively. These quite high values are comparable with data collected and modeled by Jacobson (1997) for an air pollution event in Los Angeles in 1987. With these unusually high aerosol absorption coefficients significant effects on the

Table 1
Summary of the instrumentation used in this study

Instrument	Measured quantity	Wavelength λ	Reference
Sun photometer	AOD	380–1044 nm	Ansmann et al. (2005)
Raman lidar	σ_e; σ_{BSC}	532 nm	Ansmann et al. (2005)
Nephelometer	σ_s (dry)	450; 550; 700 nm	Anderson et al. (1996)
Absorption photometer	σ_a (dry)	550; 630; 700 nm	Petzold et al. (2002)

AOD: aerosol optical depth; σ_e: volume extinction coefficient of the particles in m^{-1}; σ_s: volume scattering coefficient of the particles in m^{-1}; σ_a: volume absorption coefficient of the particles in m^{-1}; λ: wavelength in nm.

dynamics in the lower atmosphere can be expected (Zdunkowskie et al., 1976; Gray et al., 1976).

In Fig. 2 three profiles of the particle extinction coefficient (σ_e), derived from the lidar measurements, illustrate the vertical structure of the polluted PBL. The uncertainty of the retrieved extinction profiles is in the range of 10–20%. High particle extinction coefficients of up to $0.82 \times 10^{-3}\,m^{-1}$ in about 1.3 km altitude were observed in the morning hours. Furthermore, a quasi-continuous decrease of the columnar aerosol load during daytime of 23 October is obvious from the profiles in Fig. 2. This decrease is also obvious from the plots of the daytime variation of AOD and the particle scattering coefficient σ_s measured at the ground (see Fig. 3). The observed AOD values of up to 1.5 are quite remarkable. The volume scattering coefficient of the particles measured by the nephelometer at the surface reached a maximum value of roughly $0.40 \times 10^{-3}\,m^{-1}$ in the morning hours

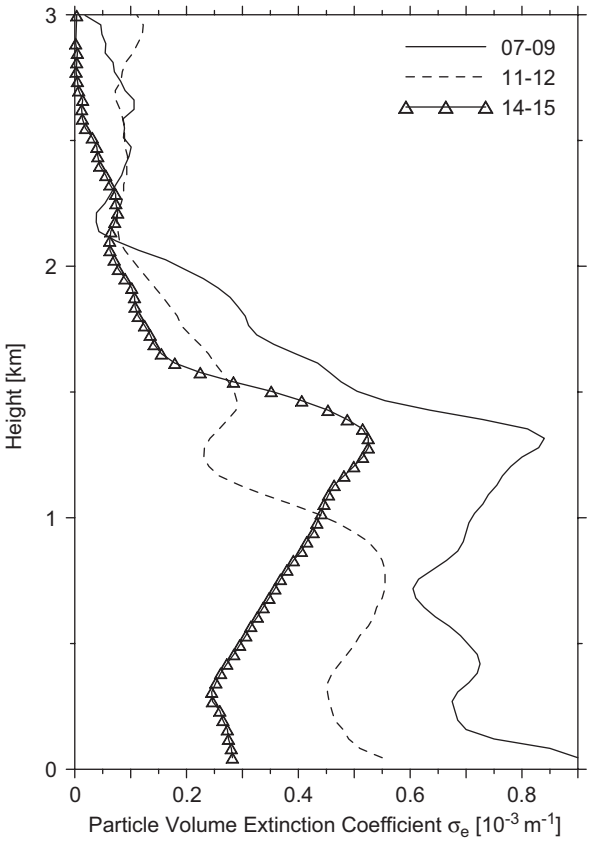

Fig. 2. Average volume extinction coefficients of particles at 532 nm wavelength, determined by lidar at Xinken, China, on 23 October 2005 for the time periods 07–09, 11–12, and 14–15 h local time.

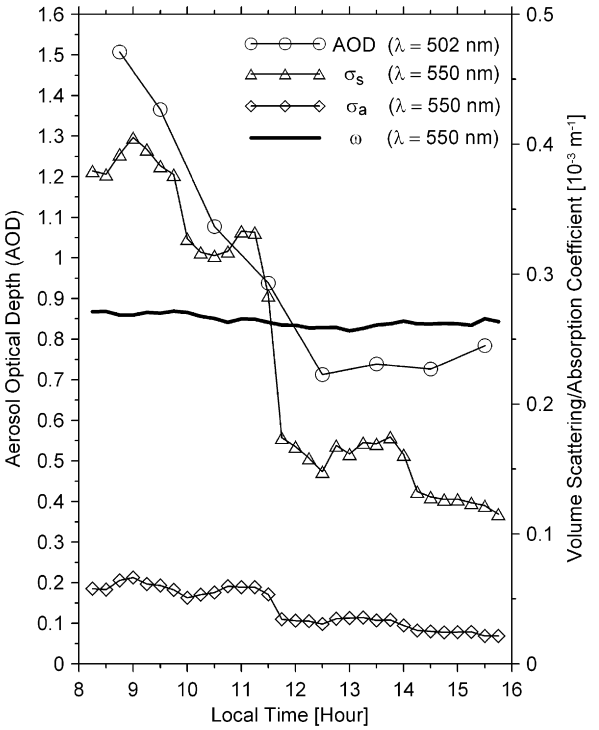

Fig. 3. Surface measurements of the diurnal variation of aerosol optical depth (AOD, at 502 nm wavelength, left scale), dry volume scattering (σ_s) and absorption (σ_a) coefficients (both at 550 nm wavelength, right scale) of the particles, and particle single-scattering albedo $\omega = \sigma_s/(\sigma_a + \sigma_s)$ (at 550 nm wavelength, left scale) as measured at Xinken, China, on 23 October 2004.

(around 9 o'clock). This value is smaller than expected from the respective profile data (07–09 local time) after extrapolation of lidar profile to the ground (see Fig. 2). This difference between the profile and the ground-based measurements of σ_s is partly explained by measurement uncertainties. Other reasons are due to the boundary layer development. There is a lack of vertical exchange in the morning. During the boundary layer development, in the course of the day, the surface measurements and the extrapolated lidar profile data converge. For example, between 14 and 15 h local time the surface value of σ_s is about $0.13 \times 10^{-3}\,m^{-1}$; the respective value from the lidar profile is quite close to the surface measurement. Best agreement between the surface and the lidar data of σ_s is achieved after full PBL development around 16–19 h local time (Eichler et al., 2006).

The maximum volume absorption coefficients σ_a measured at the surface (solid line with diamonds in Fig. 3) were in the range of $0.05 \times 10^{-3}\,m^{-1}$ and were observed in the morning hours. The resulting

single-scattering albedo ω of the dry particles remained nearly constant during the day ($\omega \approx 0.85 \pm 0.04$), indicating that the aerosol change concerned more concentrations than composition. Similar measured values of ω have been found frequently over China (Mao and Chengcai, 2005).

The in situ surface observations of particle single-scattering albedo collected on 23 October are in good agreement with indirect retrieval methods reported by Müller et al. (2006). However, the dry single-scattering albedos from the in situ observations are always in the upper range of values that were indirectly derived from the lidar, in spite of the fact that the lidar measures under ambient conditions. That would imply that the lidar-derived ambient values (including liquid water due to humidification) of the particle single-scattering albedo are higher than those from the dry in situ measurements. Müller et al. (2006) relate this fact to the influence of non-light-absorbing sea salt particles near the ground from the South China Sea and less light-absorbing dust generated by agriculture and traffic. Both sources are more important for the near-surface in situ measurements. It should also be noted that the uncertainty of the in situ values of dry particle single-scattering albedo is at least in the range of ± 0.05 (Müller et al., 2006).

2.2. Solar radiation model

The three lidar particle extinction profiles shown in Fig. 2 were used as input for the libRadtran radiative transfer model (Mayer and Kylling, 2005) to calculate the broadband-solar (in the following called solar) downward and upward irradiances ($F^{\downarrow}$, $F^{\uparrow}$) at different altitudes z from the bottom of atmosphere (BOA) to $z = 100$ km altitude (top of atmosphere, TOA). For the spectral surface albedo, data collected by Wendisch et al. (2004) over different land and sea surfaces were implemented in the simulations. For the water vapor, temperature and pressure profiles radiosonde data from Hong Kong were used. The radiative transfer calculations were conducted in time steps of 10 min for an entire diurnal solar cycle from sunrise to sunset taking into account the actual geographic location of the measurement site.

As aerosol input the profiles of the volume extinction coefficient (σ_e), the asymmetry parameter (g) and the single-scattering albedo (ω) of the particles are needed, in principle as a function of height, wavelength and time of day (i.e., solar zenith angle). For the particle volume extinction coefficient the lidar profile measurements (see Fig. 2) were projected onto the vertical model grid (mostly 100 m resolution). The spectral values of σ_e at each altitude of the vertical model grid were interpolated over the wavelength grid of the radiative transfer model using the spectral slope of the Sun photometer observations of the AOD. In order to properly represent the temporal aerosol changes in the course of the day, the three lidar particle extinction profiles from Fig. 2 were scaled and interpolated to the diurnal change of the AOD measured at 502 nm wavelength by the Sun photometer (Fig. 3). In this way, a 10-min time resolution of the profiles was achieved from the three σ_e profiles. The particle asymmetry parameter g was fixed to a value of 0.60 which is typical for a wide range of aerosol conditions (Fiebig and Ogren, 2006). For the particle single-scattering albedo the values of $\omega = 1.0$, 0.9, and 0.8 were used as free parameters which comply with the concurrent ground-based measurements. These data had indicated values around $\omega \approx 0.85$ (dried aerosol) for mid-visible wavelengths, which is supported by the study of Müller et al. (2006).

Two sets of radiation calculations were conducted. One was performed neglecting the aerosol particles and thus considering a Rayleigh atmosphere only. For these simulations the index "R" is introduced in the following text. A second set of simulations considered the scattering and absorption of both, the aerosol particles and the Rayleigh contribution due to the gas molecules (index "AP + R"). From these two sets of results of the radiative transfer simulations the so-called solar radiative forcing ΔF (in units of W m^{-2}) at the TOA and BOA was derived from the difference of net irradiances ($F^{\uparrow} - F^{\downarrow}$) at the TOA and the BOA. In particular the solar radiative forcing at TOA was calculated as follows:

$$\Delta F(\mathrm{TOA}) = [F^{\uparrow}(\mathrm{TOA})]_{\mathrm{R}} - [F^{\uparrow}(\mathrm{TOA})]_{\mathrm{AP+R}}. \quad (1)$$

The solar radiative forcing at the BOA was obtained from

$$\Delta F(\mathrm{BOA}) = [F^{\uparrow}(\mathrm{BOA}) - F^{\downarrow}(\mathrm{BOA})]_{\mathrm{R}} - [F^{\uparrow}(\mathrm{BOA}) - F^{\downarrow}(\mathrm{BOA})]_{\mathrm{AP+R}}. \quad (2)$$

A negative solar radiative forcing at the TOA (increase of solar radiation escaping to space due to aerosol particles) reduces the available solar energy for the atmosphere-surface system. Negative values of ΔF(BOA) mean a net loss of solar radiation

(i.e., a cooling) of the atmosphere and a gain of solar energy (i.e., warming) of the surface. Changes in the atmosphere alone require differencing the TOA and BOA changes in net irradiances.

From the irradiances the solar heating rate is calculated by

$$\frac{\partial T(z,t)}{\partial t} = -\frac{1}{\varrho c_p}\frac{\partial F_{net}(z)}{\partial z}, \quad (3)$$

with the temperature T, the time t, the air density ϱ and the specific heat capacity at constant pressure $c_p = 1004\,J\,kg^{-1}\,K^{-1}$, and the net irradiances $F_{net} = F^{\uparrow} - F^{\downarrow}$ as a function of altitude z.

Amongst other parameters, these results of the radiative transfer simulation (i.e., the solar upwelling and downwelling irradiance profiles) were used as off-line input to the dynamic PBL model described in the following subsection.

2.3. Dynamic PBL model

In order to study the radiatively induced aerosol effects on boundary layer meteorology the PBL height was simulated with a dynamic PBL model and compared with respective lidar measurements. In general, such a quantification of the direct aerosol impact on the temporal evolution of the PBL would require a complex dynamic three-dimensional modeling approach. A prerequisite for such an effort is the availability of the corresponding meteorological as well as physicochemical input parameters with a sufficiently high spatio-temporal resolution. Due to the lack of such data, especially the missing of mesoscale aerosol input, a more simplified one-dimensional approach is pursued here. This has been done in order to obtain a quantitative estimate of the direct radiative aerosol effect on the PBL evolution.

The chosen dynamic model is based on a third-order turbulence closure described in detail by Hellmuth (2006). The vertical model grid resolution is 40 m, the number of vertical layers is 75. The height of the Prandtl layer is fixed at 10 m. To estimate the aerosol impact on the temporal PBL height evolution in the present study, the solar radiation scheme of the columnar model by Hellmuth (2006) was replaced by the results from off-line calculations of the solar irradiances (profiles of $F^{\downarrow}$, $F^{\uparrow}$) from the radiation model (see Section 2.2). By varying the aerosol input within the solar radiation model, the respective irradiances were varied in the dynamic PBL model.

The air pollution potential of an area is directly related to two variables: (a) the vertical diffusion of pollutants represented by the mixing layer height (or the PBL height), and (b) the wind speed, averaged over the mixing layer depth, as a measure of the mean horizontal transport of pollutants. The so-called ventilation index (Holzworth, 1972) is defined as the product of these two variables (a) and (b). To evaluate the impact of the air pollution situation on the PBL evolution, this ventilation index was integrated from sunrise until a given time, which yields an accumulated ventilation index in km^2. The height of the PBL was determined using a Bulk–Richardson number approach (Holtslag et al., 1995).

The boundary layer model was dynamically forced by the prescription of a height- and time-independent geostrophic wind (with the two components $u_g = 5\,m\,s^{-1}$, $v_g = 0\,m\,s^{-1}$), whereas the x-axis of the coordinate system was aligned with downwind direction. The integration starts at 03:00 local time with an initial temperature profile for a stable boundary layer. The surface temperature, $T_0 \approx \theta_0$, was set to 288 K, whereas the lapse rate of the potential temperature, $\Gamma_\theta = \partial\theta/\partial z$, was set piecewise constant in four layers: $(\Gamma_\theta)_1 = 4\,K/100\,m$ for $z \leqslant z_p$, with z_p denoting the Prandtl layer height, $(\Gamma_\theta)_2 = 4\,K/1000\,m$ for $z_p < z \leqslant z_{inv1} = 300\,m$, $(\Gamma_\theta)_3 = 2\,K/400\,m$ for $z_{inv1} < z \leqslant z_{inv2} = 1000\,m$ with z_{inv1}, z_{inv2} being the lower and upper boundary of a free inversion, respectively, and $(\Gamma_\theta)_4 = (\Gamma_\theta)_3$ for $z_{inv2} < z$.

The initial profile of the water vapor mixing ratio was prescribed using the expression $q_v(z) = q_{v0}\exp(-z/H_{q_v})$ with $q_{v0} = 5\,g\,kg^{-1}$ denoting the surface value of the mixing ratio and $H_{q_v} = 1000\,m$ the scale height.

The temperature and humidity profiles in the free troposphere were adjusted using climatological radiosounding data from Hong Kong.

Gridscale vertical transport processes are per definition excluded in an one-dimensional model. However, large-scale subsidence can be a posteriori considered in such a model by vertical advection, described by the large-scale vertical velocity $\overline{w}$. Here, $\overline{w}$ is defined using the following expression by Hellmuth (2006, Equation B21 in Appendix B):

$$\overline{w} = \begin{cases} \overline{w}_H\left[1 - \left(1 - \dfrac{z}{H_w}\right)^{n_w}\right], & z/H_w \leqslant 1, \\ \overline{w}_H, & z/H_w > 1. \end{cases} \quad (4)$$

The parameter $\overline{w}_H$ denotes the large-scale vertical velocity at the subsidence height H_w, where the divergence of the descending air mass starts. The vertical velocity $\overline{w}_H$ was found to be the most sensitive parameter in controlling the mixing layer height. Consequently, it has been considered as a tunable parameter. The parameters entering Eq. (4) are $H_w = 1500\,\mathrm{m}$, $n_w = 2.4$, $\overline{w}_H = -0.02\,\mathrm{m\,s^{-1}}$.

To calculate the surface fluxes of momentum, heat and humidity a semi-empirical flux-partitioning scheme proposed by Holtslag (1987) is used. It solves the surface-energy budget by a simplified Penman–Monteith approach. In the scheme, both the surface-radiation budget (incoming solar radiation, reflected solar radiation from the surface, incoming longwave radiation from the atmosphere, outgoing longwave radiation from the surface) (Holtslag, 1987, Section 3, pp. 31–39) and the surface-energy budget (sensible heat flux, latent heat flux, soil heat flux, surface-radiation budget) (Holtslag, 1987, Section 4, pp. 39–47) are evaluated. The soil heat flux is parameterized in terms of the net radiation. The partitioning of the surface-energy flux (minus soil heat flux) between the sensible and latent heat flux is based on the Penman–Monteith approach. Both fluxes are parameterized in terms of net radiation and soil flux using semi-empirical parameters, adapted from observations (Holtslag, 1987, pp. 40–41). A comprehensive description of the model parameterization can be found in Hellmuth (2006, Appendix D2.2 Lower boundary conditions, Eq. D12). The most important adjustment surface parameters therein are the surface albedo α_{sfc}, the parameter c_G in $G = c_G Q^\star$, where G denotes the soil heat flux and $Q^\star$ the net radiation, as well as the surface moisture parameters α_{PM} and β_{PM} in the Penman–Monteith flux-partitioning parameterization (Holtslag, 1987, Eqs. (14) and (15), p. 40):

$$H = \frac{(1-\alpha_{\mathrm{PM}})+(\gamma/s)}{1+(\gamma/s)}(Q^\star - G) - \beta_{\mathrm{PM}},$$

$$L_{\mathrm{v}}E = \frac{\alpha_{\mathrm{PM}}}{1+(\gamma/s)}(Q^\star - G) + \beta_{\mathrm{PM}}. \qquad (5)$$

Here, H denotes the sensible heat flux and $L_{\mathrm{v}}E$ the latent heat flux, $s = \partial q_{\mathrm{s}}/\partial T$ with q_{s} being the saturation specific humidity, and $\gamma = c_{\mathrm{p}}/L_{\mathrm{v}}$, where c_{p} is the specific heat of air at constant pressure and L_{v} the latent heat of vaporization. To evaluate Eq. (5), the parameters α_{PM} and β_{PM} must be specified. Holtslag (1987) used $\alpha_{\mathrm{PM}} = 1$ and $\beta_{\mathrm{PM}} = 20\,\mathrm{W\,m^{-2}}$ for grass covered surface. These values are obtained for normal summer conditions, when the surface is supplied with enough water to evaporate. When there is lack of water the value of α_{PM} decreases. For bare soil, when there is no water to evaporate, one has $\alpha_{\mathrm{PM}} = \beta_{\mathrm{PM}} = 0$. In the present study we employed the ad hoc assumption $\alpha_{\mathrm{PM}} = 0.6$.

Owing to the third-order closure of the boundary layer model first-, second-, and third-order moments are required to initialize the model. As higher order moments are regularly not available, a spin-up phase during the model integration is necessary to ensure self-consistency between all predictive variables (no external forcing by nudging has been applied). We found that a spin-up duration of 3 h is sufficient to reach self-consistency between predictive fields. Therefore, the model is started at nighttime under very stable conditions. Thus, at sunrise the further evolution is self-consistent and mainly controlled by the radiation-induced forcing from the surface. The evolution during the daytime was found to be nearly independent of the choice of the initial profiles, except for the requirement to start with a stable stratification. Hence, in the present study the boundary layer evolution is mainly controlled by the large-scale subsidence velocity, and, to a lesser degree, by the surface albedo and surface moisture parameter. The "memory effect" of the daytime boundary evolution with respect to the nighttime initialization was found to be very small.

3. Results

3.1. Radiative effects

The exceptionally high aerosol load in the PRD observed on 23 October 2004, caused drastic radiative effects. As an example the solar radiative forcing of the aerosol particle is plotted in Fig. 4 as a function of the time of day.

The solar radiative forcing in general is negative, i.e., the particles reduce the solar energy within the atmosphere-surface system. For the observed particle single-scattering albedo of $\omega = 0.85$ solar aerosol radiative effects of up to $-49\,\mathrm{W\,m^{-2}}$ at the TOA (see Fig. 4a) and $-219\,\mathrm{W\,m^{-2}}$ at the BOA (see Fig. 4b) are simulated with the radiative transfer model around 09 local time. Averaging over the sunlit part of the day still yields $-160\,\mathrm{W\,m^{-2}}$ solar radiative forcing at the BOA

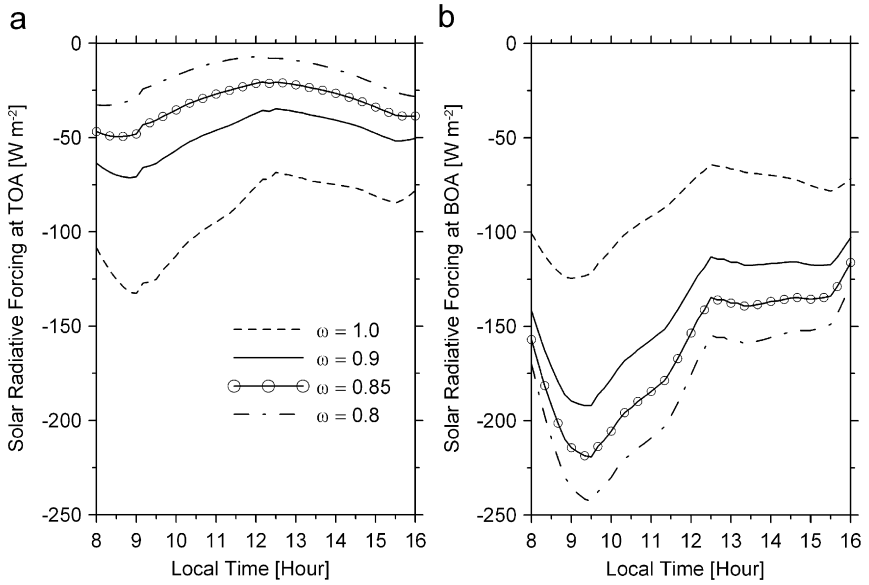

Fig. 4. Diurnal cycle of the simulated solar radiative forcing at the top of atmosphere (a: left panel, see Eq. (1)) and at the bottom of the atmosphere (b: right panel, see Eq. (2)) for different values of the particle single-scattering albedo ω at Xinken, China, on 23 October 2004.

($\omega = 0.85$). Increasing particle absorption (decreasing ω) in general reduces the solar aerosol radiative effects at the TOA and increases the absolute solar aerosol forcing at the BOA. The aerosol layer absorbs up to 31% (daily average, $\omega = 0.8$) of the solar radiation incident at the top of the layer for the situation reported here. For low Sun the aerosol-induced absorption reaches values up to 59%. These are, to our knowledge the largest aerosol effects on solar radiation ever reported in literature.

From the irradiance profiles the solar heating rates were calculated via Eq. (3). In Fig. 5a both aerosol particle and Rayleigh (gas molecules) scattering and absorption are included, in Fig. 5b the Rayleigh contribution is subtracted. The results of the simulations are shown for the observed particle single-scattering albedo of $\omega = 0.85$. The aerosol particles cause a substantial warming with maximum values at the top of the aerosol layer (see Fig. 2) of up to 7–8 K day^{-1} (see Fig. 5b). This warming causes the atmospheric stratification getting more stable.

Solar heating rate values caused by aerosol particles alone of about 6 K day^{-1} (0.25 K h^{-1}) have been published by Jacobson (1997). Even larger heating rates (up to 24 K day^{-1}) were reported by Pilewskie and Valero (1992), and Hobbs and Radke (1992) for the exceptional event of the Kuweit oil fires. Additionally these authors report AODs of 2–3, and particle single-scattering albedos of 0.5–0.6. However, these values exerted only local radiative effects, because the smoke was not carried high in the atmosphere and only present for a short time period. Instead, the high load of absorbing aerosol particles in China is a long-term problem with relevance to larger areas.

The solar heating due to the absorbing particles is not counterbalanced by the terrestrial cooling. This is clearly shown in Fig. 6 which compares the solar heating rates (Fig. 6a) with the respective terrestrial cooling rates (Fig. 6b) for different values of particle single-scattering albedo ω. The solar heating rates are derived from the solar radiation model, terrestrial cooling rates were obtained from the dynamic PBL model. The temperature change rates are shown for the time period with the largest solar radiative effects (around 09 local time; see Fig. 4). Most of the solar heating occurs at the top of the PBL, which causes the stabilizing effect. With increasing particulate absorption (decreasing ω) the aerosol stabilizes PBL stratification further and thus reduces convective mixing and PBL heights.

In case of non-absorbing particles ($\omega = 1$), the atmosphere still cools down at the time of day considered in this case (07–09 local time). As soon as some absorption is assumed for the particles the upper parts of the aerosol layers (see Fig. 2) are effectively warmed.

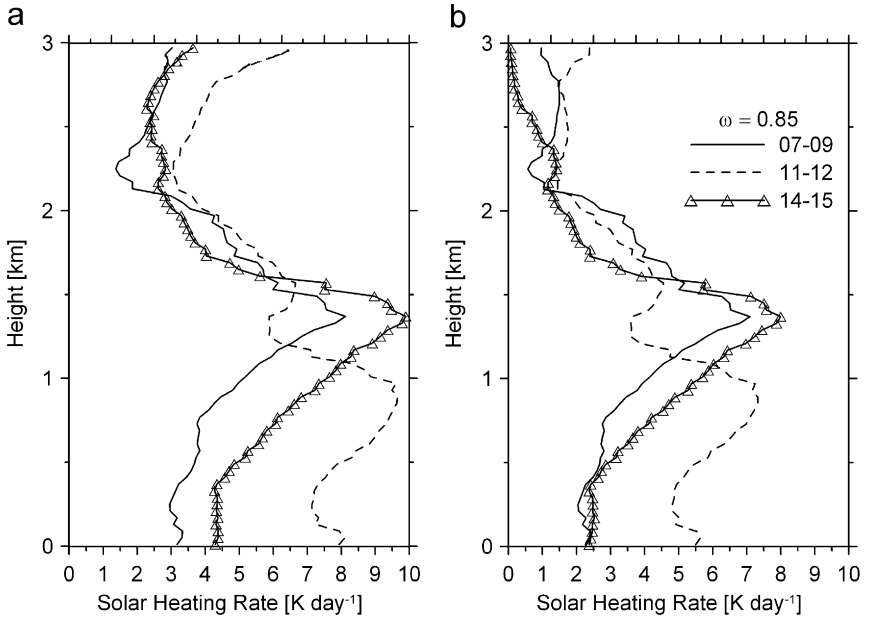

Fig. 5. Profiles of solar heating rate for the time periods 07–09, 11–12, and 14–15 local time for a value of the particle single-scattering albedo $\omega = 0.85$ at Xinken, China, on 23 October 2004. The left panel shows the total solar heating rates, the right panel depicts the heating rates due to aerosol particles only.

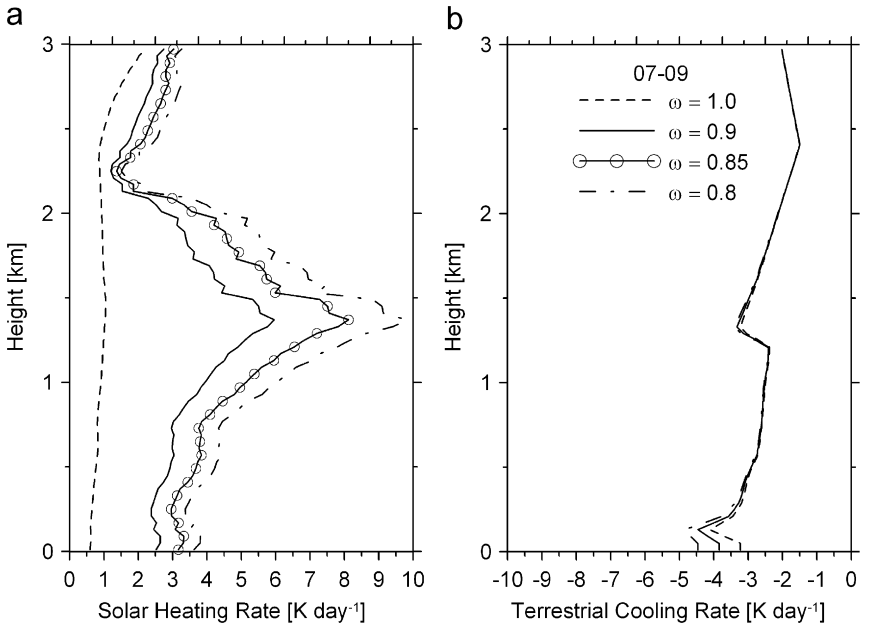

Fig. 6. Average solar heating (a: left panel, Aerosol + Rayleigh similar to Fig. 5a) and terrestrial cooling (b: right panel) rate profiles for the time periods 07–09 local time for different values of the particle single-scattering albedo ω at Xinken, China, on 23 October 2004.

3.2. *Effects on temporal PBL evolution*

Driven by the solar heating of the surface and the adjacent air boundary layer, the height of the PBL usually rises dynamically in the course of the day to values of between 1 and 2.5 km height in the afternoon. This has been confirmed by the lidar measurements presented in Fig. 7 (solid line with

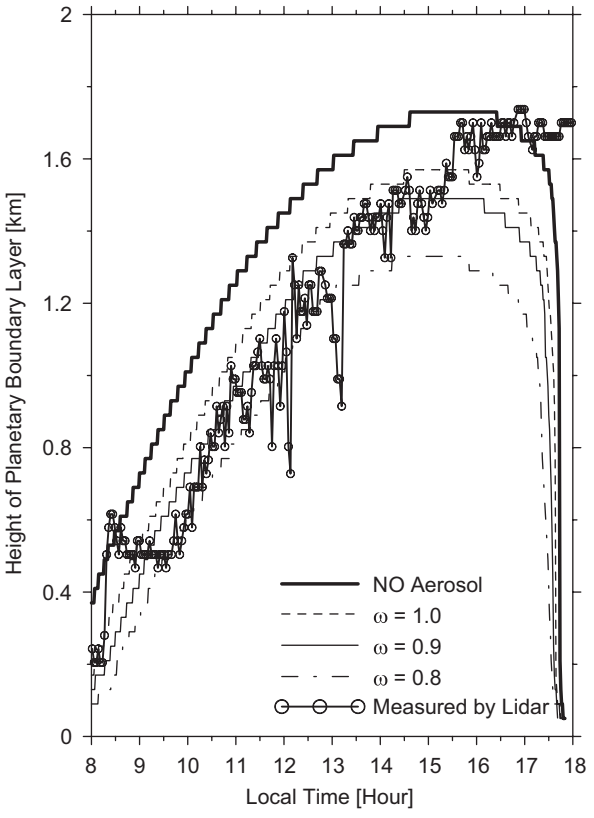

Fig. 7. Modeled PBL (planetary boundary layer) heights without aerosol ("NO Aerosol"; thick solid line), and with aerosol and dry particle single-scattering albedos ω of 1.0, 0.9 and 0.8. The measured PBL height is marked by a thin solid line with circles.

circles). Here in the afternoon a PBL height of about 1.5 km is observed.

In order to reproduce these PBL-height lidar measurements, the PBL model described in Section 2.3 was applied. The PBL model was directly driven by the simulated solar irradiances from the radiation model (cf. Section 2.2). A sensitivity study was performed as follows: At first, the PBL model was empirically adjusted to the observed lidar-based PBL height by varying the Bowen ratio and the large-scale subsidence velocity within realistic ranges. In this way, both the model setup and the reference scenario were defined. Secondly, the sensitivity of the predicted PBL height against the aerosol-induced radiative forcing was investigated. The lidar observations gave no hint on a substantial impact of the daytime sea breeze on the PBL height evolution. Therefore the present approach is appropriate to get quantitative results on the mean dynamic effect of the PBL aerosols, averaged over a densely populated area.

The results of the dynamic PBL modeling are compared in Fig. 7 (step curves indicate modeled PBL heights) with the respective measurements (solid line with circles). The modeled PBL heights rise to roughly 1.3–1.7 km altitude at about 14:00–16:00; in the late afternoon the modeled PBL heights start decreasing which is caused by the decline of solar heating of the surface and boundary layer due to the setting Sun. The measured values follow the increasing trend of the modeled PBL heights until roughly 15:30. However, the measured PBL heights do not drop in the late afternoon; instead they abruptly increase. This sudden increase after 15:30 is caused by slight cloud development starting at that time. This cloud evolution is not captured by the model (which does not consider clouds at all) and thus the modeled PBL heights differ from the respective measurements in the late afternoon. On the other hand, the lidar-derived PBL height in the late afternoon and early evening generally shows the fully developed daytime haze layer. The modeled PBL height can no longer be identified by an aerosol backscatter lidar (when the PBL convection breaks down).

In general, Fig. 7 shows that the absorbing aerosol particles decrease the PBL height systematically due to their solar heating capacity and in turn their stabilizing effects within the PBL. This stabilization has severe effects on the ventilation of the polluted PBL and may also suppress or delay convective cloud formation on many days with moist conditions close to the top of PBL. The ventilation is quantified by the accumulated ventilation index V (for explanation see Section 2.3). Relative to a PBL without aerosol particles, V is reduced to values around 30% for $\omega = 0.8$ in the morning hours. When PBL heights stabilize in the afternoon the accumulated ventilation index assumes values of 85%, 79%, and 67% of the aerosol-free ventilation for $\omega = 1.0$, 0.9, and 0.8, respectively.

The study by Rudich et al. (2003) observed cloud evolution above an extremely absorbing aerosol layer (Kuweit oil fires). These authors report that the cloud formation in their case was caused by convection above the aerosol layer which was triggered by local heating. The triggering was clearly due to the absorbing aerosol particles (not by surface heating). The absorption of solar radiation heats the aerosol-laden air, which therefore is forced to ascend. During the ascend the air cools and as a consequence clouds evolve. However, the Kuweit oil fires were a truly exceptional event with mostly regional impact.

Particle single-scattering albedos were around 0.5, optical thickness reached values of 2–3 (Pilewskie and Valero, 1992; Hobbs and Radke, 1992). In our case we have observed higher values of single-scattering albedo of the particles and optical thickness values were in the range of 1; the heating rates reached values of up to 5 K day^{-1} (in the Kuweit oil fires values of up to 25 K day^{-1} were reported, Pilewskie and Valero, 1992). Therefore the heating of the air in the aerosol-laden boundary layer was lower in our case and thus aerosol absorption-induced convection is much less likely in our case.

4. Conclusions

Over the densely populated and highly polluted Pearl River Delta (PRD), China, extremely high aerosol optical depths (0.5–1.5 at 502 nm wavelength) within the boundary layer lead to losses of solar radiation at the surface of up to 40%. During the course of the day, this highly absorbing aerosol heats up the first kilometer of the atmosphere to an extent that reduces the ventilation of the air pollution by more than 30%. This, in turn implies an increase of pollutant concentration of about 30%. This meteorological consequence of the particulate pollution aggravates the pollution problems for the population and vegetation exposed to it. Whereas the elimination of absorbing aerosol particles would yield a positive effect on boundary layer ventilation (cf. Fig. 7, curve "NO Aerosol") the most effective means to reduce aerosol-reduced ventilation of air pollution should focus on the black carbonaceous aerosol fraction which only comprises about 12% in terms of mass concentration in the PRD in order to break this feedback between aerosol pollution and its ventilation. There are several other regions with highly absorbing particulate pollution where similar ventilation feedbacks can be expected: the urban areas of Beijing (Zheng et al., 2005) and New Delhi (Gurjar et al., 2004), regions of extremely high biomass burning, e.g., over the dry Amazonian area (Schafer et al., 2002), and continental pollution plumes such as over the Eastern seaboard of the U.S. (Russell et al., 1999) and over and downwind of South Asia (Ramanathan et al., 2005).

Acknowledgments

Matthias Tesche is gratefully thanked for his comments on the manuscript. This study was supported by China National Basic Research and Development Programs 2002CB410801 and 2002CB211605.

References

Ackerman, A.S., et al., 2000. Reduction of tropical cloudiness by soot. Science 288, 1042–1047.

Althausen, D., Engelmann, R., Foster, R., Rhone, P., Baars, H., 2004. Portable Raman lidar for determination of particle backscatter and extinction coefficients. In: Pappalardo, G., Amodeo, A. (Eds.), Reviewed and Revised Papers Presented at the 22nd ILRC, ESA SP-561, vol. 1. ESA Publications Division, ESTEC, Noordwijk, The Netherlands, pp. 83–86.

Anderson, T.L., et al., 1996. Performance characteristics of a high-sensitivity, three-wavelength, total scatter/backscatter nephelometer. Journal of Atmospheric and Oceanic Technology 13, 967–986.

Ansmann, A., et al., 2005. High aerosol load over the Pearl River Delta, China, observed with Raman lidar and Sun photometer. Geophysical Research Letters 32, L13815.

Brooks, I.M., 2003. Finding boundary layer top: application of a wavelet covariance transform to lidar backscatter profiles. Journal of Atmospheric and Oceanic Technology 20, 1092–1105.

Chung, C.E., Ramanathan, V., Kiehl, J.T., 2002. Effects of the south Asian absorbing haze on the northeast monsoon and surface-air heat exchange. Journal of Climate 15, 2462–2476.

Eichler, H., Cheng, Y.F., Birmili, W., Wiedensohler, A., Brüggemann, E., Gnauk, T., Herrmann, H., Althausen, D., Ansmann, A., Engelmann, R., Tesche, M., Zhang, Y.-H., Hu, M., Liu, S., Zeng, L.M., 2006. Hygroscopic properties and ambient extinction of aerosol particles in South-Eastern China. Atmospheric Environment, submitted for publication.

Fiebig, M., Ogren, J.A., 2006. Retrieval and climatology of the aerosol asymmetry parameter in the NOAA aerosol monitoring network. Journal of Geophysical Research 111, D21204.

Gray, W.M., Frank, W.M., Corrin, M.L., Stokes, C.A., 1976. Weather modification by carbon dust absorption of solar energy. Journal of Applied Meteorology 15, 155–186.

Gurjar, B.R., Aardenne, J.A.v., Lelieveld, J., Mohan, M., 2004. Emission estimates and trends (1990–2000) for megacity Delhi and implications. Atmospheric Environment 38, 5663–5681.

Hellmuth, O., 2006. Columnar modelling of nucleation burst evolution in the convective boundary layer—first results from a feasibility study. Part I: modelling approach. Atmospheric Chemistry and Physics 6, 4175–4214.

Hobbs, P.V., Radke, L.F., 1992. Airborne studies of the smoke from Kuweit oil fires. Science 256, 987–991.

Holtslag, A.A.M., 1987. Surface fluxes and boundary layer scaling. Models and applications. Scientific Report WR 87-2 (FM), Koninklijk Nederlands Meteorologisch Instituut (KNMI).

Holtslag, A.A.M., van Meijgaard, E., De Rooy, W.C., 1995. A comparison of boundary layer diffusion schemes in unstable conditions over land. Boundary-Layer Meteorology 76, 69–95.

Holzworth, G.C., 1972. Office of Air Publication No. AP-101, O. o. A. P. US Environmental Protection Agency, Research Triangular Park, NC, US.

Jacobson, M.Z., 1997. Development and application of a new air pollution modeling system—part III. Aerosol phase simulations. Atmospheric Environment 31, 587–608.

Jacobson, M.Z., 1998. Studying the effects of aerosols on vertical photolysis rate coefficient and temperature profiles over an urban airshed. Journal of Geophysical Research 103, 10593–10604.

Jacobson, M.Z., Kaufman, Y.J., 2006. Wind reduction by aerosol particles. Geophysical Research Letters 33, L24814.

Krishnan, R., Ramanathan, V., 2002. Evidence of surface cooling from absorbing aerosols. Geophysical Research Letters 29.

Lammert, A., Bösenberg, J., 2005. Determination of the convective boundary-layer height with laser remote sensing. Boundary-Layer Meteorolology 119, 159–170.

Mao, J., Chengcai, L., 2005. Observation study of aerosol radiative properties over China. Acta Meteorologica Sinica 63, 622–635.

Martucci, G., Matthey, R., Mitev, V., Richter, H., 2007. Comparison between backscatter lidar and radiosonde measurements of the diurnal and nocturnal stratification in the lower troposphere. Journal of Atmospheric and Oceanic Technology 24, 1231–1244.

Mayer, B., Kylling, A., 2005. Technical note: the libRadtran software package for radiative transfer calculations—description and examples of use. Atmospheric Chemistry and Physics 5, 1855–1877.

Menon, S., Hansen, J., Nazarenko, L., Luo, Y.F., 2002. Climate effects of black carbon aerosols in China and India. Science 297, 2250–2253.

Müller, D., Tesche, M., Eichler, H., Engelmann, R., Althausen, D., Ansmann, A., Cheng, Y.F., Zhang, Y.H., Hu, M., 2006. Strong particle light absorption over the Pearl River Delta (south China) and Beijing (north China) determined from combined Raman lidar and Sun photometer observations. Geophysical Research Letters 33.

Petzold, A., Kramer, H., Schönlinner, M., 2002. Continuous measurement of atmospheric black carbon using a multi-angle absorption photometer. Environmental Science and Pollution Research 4, 78–82.

Pilewskie, P., Valero, F.J., 1992. Radiative effects of the smoke clouds from the Kuweit oil fires. Journal of Geophysical Research 97, 14541–14544.

Podgorny, I.A., Conant, W., Ramanathan, V., Satheesh, S.K., 2000. Aerosol modulation of atmospheric and surface solar heating over the tropical Indian Ocean. Tellus 52B, 947–958.

Ramanathan, V., Ramana, M.V., 2005. Persistent, widespread, and strongly absorbing haze over the Himalayan foothills and the Indo-gangetic plains. Pure and Applied Geophysics 61, 1609–1626.

Ramanathan, V., Crutzen, P.J., Kiehl, J.T., Rosenfeld, D., 2001. Aerosols, climate, and the hydrological cycle. Science 294, 2119–2124.

Ramanathan, V., et al., 2005. Atmospheric brown clouds: impacts on south Asian climate and hydrological cycle. Proceedings of the National Academy of Sciences of the USA 102, 5326–5333.

Rudich, Y., Sagi, A., Rosenfeld, D., 2003. Influence of the Kuweit oil fire plume (1991) on the microphysical development of clouds. Journal of Geophysical Research 108.

Russell, P.B., et al., 1999. Aerosol-induced radiative flux changes off the United States Mid-Atlantic coast: comparison of values calculated from sunphotometer and in situ data with those measured by airborne pyranometer. Journal of Geophysical Research 104, 2289–2307.

Schafer, J.S., Holben, B.N., Eck, T.F., Yamasoe, M.A., Artaxo, P., 2002. Atmospheric effects on insolation in the Brazilian Amazon: observed modification of solar radiation by clouds and smoke and derived single scattering albedo of fire aerosols. Journal of Geophysical Research 107 LBA 41-1–41-15.

Wendisch, M., et al., 2004. Airborne measurements of areal spectral surface albedo over different sea and land surfaces. Journal of Geophysical Research 109.

Zdunkowskie, W.G., Welch, R.M., Paegle, J., 1976. One-dimensional numerical simulation of the effects of air pollution on the planetary boundary layer. Journal of Atmospheric Science 33, 2399–2414.

Zhang, Y.H., Hu, M., Zhong, L.J., Wiedensohler, A., Liu, S., Andreae, M., Wang, W., Fan, M., 2007. Regional integrated experiments of air quality over Pearl River Delta 2004: overview. Atmospheric Environment, submitted for publication.

Zhao, C., Tie, X., Lin, Y., 2006. A possible positive feedback reduction of precipitation and increase in aerosols over eastern China. Geophysical Research Letters 33, L11814.

Zheng, M., et al., 2005. Seasonal trends in PM2.5 source contributions in Beijing, China. Atmospheric Environment 39, 3967–3976.